BIOCHEMISTRY
including biophysical chemistry & molecular biology

Article

pubs.acs.org/biochemistry

Residue-Dependent Thermodynamic Cost and Barrel Plasticity Balances Activity in the PhoPQ-Activated Enzyme PagP of *Salmonella typhimurium*

Bharat Ramasubramanian Iyer and Radhakrishnan Mahalakshmi*

Molecular Biophysics Laboratory, Department of Biological Sciences, Indian Institute of Science Education and Research, Bhopal 462023, India

Supporting Information

ABSTRACT: PagP is an eight-stranded transmembrane β-barrel enzyme indispensable for lipid A palmitoylation in Gram-negative bacteria. The severity of infection by pathogens, including *Salmonella*, *Legionella*, and *Bordetella*, and resistance to antimicrobial peptides, relies on lipid A remodeling by PagP, rendering PagP a sought-after drug target. Despite a conserved sequence, more robust palmitoylation of lipid A is observed in *Salmonella typhimurium* compared to *Escherichia coli*, a possible consequence of the differential regulation of PagP expression and/or specific activity. Work here identifies molecular signatures that demarcate thermodynamic stability and variances in catalytic efficiency between *S. typhimurium* (PagP-St) and *E. coli* (PagP-Ec) transmembrane PagP barrel variants. We demonstrate that *Salmonella* PagP displays a 2-fold destabilization of the barrel, while achieving 15−20 magnitude higher lipase efficiency, through subtle alterations of lipid-facing residues distal from the active site. We find that catalytic properties of these homologues are retained across different lipid environments such as micelles, vesicles, and natural extracts. By comparing thermodynamic stability with activity of selectively designed mutants, we conclude that activity−stability trade-offs can be influenced by factors secluded from the catalytic region. Our results provide a compelling correlation of the primary protein structure with enzymatic activity, barrel thermodynamic stability, and scaffold plasticity. Our analysis can open avenues for the development of potent pharmaceuticals against salmonellosis.

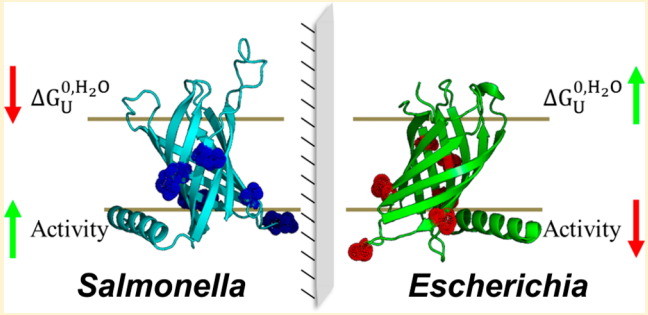

Pathogenic Gram-negative salmonellae are causative agents of debilitating (and often fatal) gastroenteritis, systemic febrile disease, diarrhea, typhoid fever, and food poisoning, with long-term effects including reactive arthritis, chronic arthritis, and other severe illnesses.[1−4] Salmonellosis is one of the most prevalent infections (>1.2 million infected solely in the United States[5]), with deaths from typhoid fever worldwide placed at >200 000 every year.[5] Bacterial resistance to antimicrobial peptides, free radical and acid stress, host immuno-evasion, crucial to *Salmonella* replication and pathogenesis, is primarily mediated by the virulence system PhoPQ.[6−8] The PhoPQ regulon is involved in bacterial infection, adaptive response to host stress factors and nutrient depletion, and macrophage survival.[7,8] One of the players in the PhoPQ two-component system is the PhoPQ-activated outer membrane (OM) lipid A palmitoyltransferase enzyme PagP (PhoP/PhoQ-activated gene P).

PagP is distributed in certain Gram-negative bacteria, including *Yersinia*, *Bordetella*, *Pseudomonas*, and *Escherichia* genomes, with homologues of this protein responsible for the virulence of *Bordetella* and *Legionella*.[6,9−15] It modifies the lipid A component of the lipopolysaccharide by palmitoylation,[16] thereby antagonizing endotoxin signaling as well as conferring resistance to cationic antimicrobial peptides.[17] This is achieved when PagP precisely transfers a 16-carbon saturated palmitoyl chain from phospholipids to lipopolysaccharides. Lipid A modification has been reported in *Pseudomonas*-infected cystic fibrosis patients.[18] Specifically, during septic shock in *Salmonella* infection, considerable palmitoylation of lipid A is commonly observed.[13,19] PagP is also essential for membrane repair in *Salmonella*.[6] Hence, the nature and efficacy of the host innate immune response to infection are dependent on the structural component of lipid A, which in turn is determined by PagP. It is therefore strongly believed that the design of potent drug inhibitors of PagP is critical to suppressing infection by bacterial pathogens, including *Salmonella*.[13] Such design would require a complete understanding of the factors that control PagP barrel structure, folding and function, at the molecular level.

Unlike other eight-stranded OM barrels that form closed structures, NMR and crystal structures of *E. coli* PagP together revealed a considerably tilted, lipid solvated barrel for PagP.

Received: May 19, 2015
Revised: September 1, 2015
Published: September 3, 2015

DOI: 10.1021/acs.biochem.5b00543
Biochemistry 2015, 54, 5712−5722

This structure displays not only shortened strands[10,15,20−22] but also weakened hydrogen bonds at the two laterally positioned faces of the folded structure.[23,24] These faces form the crenel and molecular embrasure in the protein for ingress and egress of the phospholipid donor and lipid A acceptor, respectively, through lateral diffusion.[21,24] Further, the protein also possesses an N-terminal amphipathic α-helix, which serves as the post-assembly clamp,[25] anchoring the protein to the membrane and facilitating enzymatic activity even under external stress.

In *E. coli* PagP (PagP-Ec), precise selection of the 16-carbon lipid during catalysis is achieved by an internal hydrocarbon ruler situated within the barrel.[20,21,26,27] Evidently, functioning and specificity of PagP in pathogens where this protein is functional are critically dependent on retaining a proper tilt and fold of the protein, in an OM leaflet that is particularly prone to considerable change in lipid composition during infection.[17,28,29] It has also been observed that this enzyme displays differential dynamics to facilitate substrate binding and catalysis.[21,23] Molecular factors that confer such structure, stability, and flexibility to PagP are still less understood; it is therefore of utmost importance to understand hidden residue-based signatures in this enzyme.

A recent finding identified *S. typhimurium* PagP (PagP-St) and PagP-Ec as bifunctional palmitoyltransferases, which target both lipid A and phosphatidylglycerol.[30] PagP variants from several sources show a highly conserved primary sequence, particularly at the active site. Considering known variations in lipid A palmitoylation, modulation of PagP activity in a species-dependent manner by distal signature residues is therefore highly plausible. Identifying and characterizing such critical variances that may be responsible for functional differences in palmitoylation between PagP-St and PagP-Ec are crucial for rational drug development. In this study, we provide compelling evidence for a residue-specific influence on thermodynamic stability and enzymatic activity, arising from barrel plasticity, in the two PagP forms from *S. typhimurium* and *E. coli*. We purport this difference in PagP-St as a lucrative Achilles heel for drug targeting.

MATERIALS AND METHODS

Molecular Dynamics Simulations. All molecular dynamics (MD) simulations were performed at a constant temperature of 310 K and a constant pressure of 1 bar, using GROMACS v5.0.4.[31] On the basis of a previous study,[32] we obtained the pre-oriented crystal structure of PagP-Ec (PDB ID 1THQ[20]) from the OPM database[33] and embedded this in a micelle consisting of 80 *n*-dodecylphosphocholine (DPC) molecules, >14000 water molecules and 3 K^+ ions, using the CHARMM-GUI[34−36] input generator (Supporting Information Table S1). The TIP3P model of water was used to solvate the system, and potassium ions were added to balance the charges on the protein surface. An energy minimization step and six subsequent steps of equilibration were performed, during which the protein molecule was restrained. Once the protein−micelle complex was equilibrated, all positional restraints were removed, and a production MD simulation of 10 ns was performed. In the case of PagP-St, the starting protein structure was generated by computationally mutating the pre-oriented crystal structure of PagP-Ec at each position of difference using CHARMM-GUI input generator. The subsequent simulation steps were the same as described for PagP-Ec.

Reagents and Chemicals. All ultrapure chemicals were procured from Sigma-Aldrich Co. LLC., enzymes from New England Biolabs, Inc., chromatography columns from GE Healthcare Life Sciences, and lipids from Avanti Polar Lipids, Inc.

Protein Production and Mutant Generation. The *pagP* gene was PCR-amplified from the genomes of *E. coli* and *S. typhimurium* without the signal sequence and cloned into pET3a vector (Novagen/EMD Millipore Chemicals). PagP-Ec and PagP-St (PagP proteins from *E. coli* and *S. typhimurium*, respectively) were expressed as inclusion bodies, using reported protocols.[37,38] All mutants described in this study were generated by site-directed mutagenesis and expressed as inclusion bodies. The proteins were purified under denaturing conditions in 8.0 M urea, on an anion exchange column and stored after dialysis as lyophilized powders.

Refolding in Lipid Vesicles and DPC Micelles. Refolding in small unilamellar vesicles of 1,2-dilauroyl-*sn*-glycero-3-phosphocholine (DLPC; 12:0 PC), 1,2-dimyristoyl-*sn*-glycero-3-phosphocholine (DMPC; 14:0 PC), 1,2-dihexadecanoyl-*sn*-glycero-3-phosphocholine (DPPC; 16:0 PC), 1,2-dioctadecanoyl-*sn*-glycero-3-phosphocholine (DSPC, 18:0 PC), or *E. coli* total lipid extract was carried out using a modified version of a previously reported protocol.[25] Briefly, denatured PagP (8.0 μg/μL in 8 M guanidine hydrochloride (GdnHCl)) was 100-fold diluted into a final concentration of 5 mM lipid vesicles (2.5 mg/mL in the case of total lipid extract) in 50 mM phosphate buffer pH 8.0 containing 7 M urea, at 25 °C, and incubated at 25 °C for 1 h and ∼12 h. Folding efficiency was assessed by SDS-PAGE gel mobility shifts of unboiled samples.[25,37] The final protein concentration of 0.08 μg/μL (∼4.2 μM) thus obtained corresponded to a lipid-to-protein ratio of ∼1200:1. Additionally, PagP was also refolded in 10 mM DLPC using the same protocol, to obtain a final refolded protein concentration of 0.16 μg/μL and a DLPC-to-protein ratio of ∼1200:1.

For refolding in DPC, denatured PagP (6.0 μg/μL in 8.0 M urea) was 10-fold diluted into the refolding reaction containing 100 mM DPC micelles in 20 mM Tris-HCl pH 9.5. Following this, a heat shock at 70 °C was administered for 3 min,[37] followed by an ∼12 h incubation at 4 °C, to obtain the refolded protein stock (checked using SDS-PAGE). Stock concentrations were adjusted to 0.6 μg/μL refolded PagP (∼0.03 mM) in 100 mM DPC for use in all experiments. This concentration corresponded to a detergent-to-protein ratio of ∼3200:1.

Pulse Proteolysis. Pulse proteolysis using proteinase K was carried out using minor modifications of reported protocols.[37,39] Briefly, proteinase K (PK) or PK buffer (control) was added to the refolding reaction containing ∼0.3 μg/μL PagP in 50 mM DPC and 20 mM Tris-HCl pH 9.5, and incubated at 37 °C for 1−2 min. The final concentration of PK was maintained at 0.2 μg/μL for all samples and examined on SDS-PAGE gels.

pNPP Assay to Monitor Enzymatic Activity. The catalytic activity of PagP refolded in lipid vesicles (DLPC, DMPC, DPPC, DSPC, and *E. coli* total lipid extract) and DPC was monitored by performing a modified version of the well-established standard lipase assay using the substrate analog *p*-nitrophenyl palmitate (*p*NPP).[25,40] In a final volume of 150 μL (0.02 μg/μL protein), 1.0 μM protein was added to the assay mixture consisting of 1 mM substrate, 1.2 mM lipid (0.6 mg/mL in the case of total lipid extract) and 2% Triton X-100 in 50 mM phosphate buffer pH 8.0. In the case of DPC-refolded PagP, the final protein and detergent concentrations were maintained at 2.0 μM and 10 mM, respectively, in 20 mM Tris-HCl pH 9.5. Activity was detected by measuring the absorbance

DOI: 10.1021/acs.biochem.5b00543
Biochemistry 2015, 54, 5712−5722

at 405 nm, which indicated the formation of the hydrolysis product *p*-nitrophenol, after a likely transfer of palmitate to Triton-X-100.[25,30,40] The rate of the reaction was monitored for 90−180 min, and enzyme activity was calculated in nmol/min/μM protein, using the initial linear segment of the kinetics plot.

Spectroscopic Measurements. All spectroscopic measurements were performed at 25 °C using a protein concentration of 0.06 μg/μL unless otherwise mentioned. In all cases, refolded protein solution contained 0.08 M urea and 10 mM DPC in 20 mM Tris-HCl pH 9.5 (10-fold dilution of the stock protein), whereas the unfolded protein sample was prepared in 8.0 M GdnHCl or urea.

Steady state fluorescence emission scans were recorded between 310 and 400 nm, at data intervals of 0.5 nm, using a λ_{ex} of 295 nm for tryptophan. The excitation and emission slit widths were maintained at 2.5 and 3.0 nm, respectively. All data were corrected for dark counts. Far-UV circular dichroism (CD) wavelength scans were recorded using a 5 mm quartz cuvette, between 207 and 260 nm at a temperature of 5 °C. Scan speeds were set to 100 nm/min, with a 1 nm bandwidth and data integration time of 1.0 s. Data were averaged over three accumulations, subtracted for blank and smoothened, and converted to molar ellipticity (ME) values.[37]

For acrylamide quenching experiments, samples were incubated with 0.05−0.5 M acrylamide for 5 min in the dark. Data were recorded using a λ_{ex} of 295 nm and a $\lambda_{em\text{-}max}$ of 342 and 360 nm for folded and unfolded protein samples, respectively. Data were fitted to the Stern−Volmer equation[41] and the quenching constant (K_{SV}) was derived.[42]

Tryptophan lifetime ($<\tau>$) measurements were performed using the time-correlated single photon counting at a λ_{ex} = 295 nm and a $\lambda_{em\text{-}max}$ of 342 and 360 nm for folded and unfolded protein samples, respectively. Data were fitted to a three-state exponential function, and the average lifetime was calculated from the fits.[41]

Equilibrium Unfolding and Refolding. Equilibrium unfolding/refolding experiments were carried out between ∼0.7 M and ∼ 8.0 M GdnHCl at 25 °C. (Un/Re)folded PagP containing 0.8 M urea, 100 mM DPC, 20 mM Tris-HCl pH 9.5, with or without ∼8.0 M GdnHCl, was 10-fold diluted into a GdnHCl gradient, while maintaining the final protein and DPC concentrations at 0.06 μg/μL and 10 mM, respectively. The progress of the reaction was monitored for 48 h using Trp fluorescence at 320−400 nm, using a λ_{ex} of 295 nm. Trp anisotropy (r) was recorded at the end point.

Unfolded fractions were calculated from fluorescence data at 342 nm and thermodynamic parameters (equilibrium free energy of folding (ΔG^0_U), m value, midpoint of chemical denaturation (C_m)) were derived from fits of the data to a two-state equation.[43,44] Anisotropy data were fitted to a sigmoidal function and only $C_{m\text{-}r}$ (anisotropy C_m) values were considered.

Thermal Denaturation. Protein denaturation and recovery with temperature were monitored using far-UV CD. Thermal melts of 0.06 μg/μL protein in 10 mM DPC were monitored between 5 and 95 °C and 95−5 °C, using ramp rates of 1 °C/min, at wavelengths of 215 and 231 nm. All CD data were converted to ME values,[37] and linear segments of the ME_{231} data were fitted to a linear equation,[45] and the "$T_{m\text{-start}}$" temperature thus obtained was used as an indicator of the stability of each protein. Near-UV CD wavelength scans were obtained for the same temperature range at steps of 5 °C, between 210 and 280 nm. All data were corrected for blank and smoothened.[37]

Database and Covariance Analyses. Multiple sequence alignment read-out of 610 PagP sequences from the Pfam database (pfam.sanger.ac.uk) was manually curated to include only those bacterial sources relevant to humans, for purposes of simplicity. The 556 sequences thus obtained were analyzed for residue propensity at positions 57, 91 and others, and classified based on their occurrence in pathogenic, mildly pathogenic, or nonpathogenic bacteria. Bacterial strains causing fatal or chronic illness in humans were classified as pathogenic, whereas strains which lead to medical conditions that can be cured were termed as mildly pathogenic. Finally, bacteria that do not cause any adverse pathological condition in the human host were considered to be nonpathogenic. Additionally, the active site residues (H, D, and S) positioned at 33, 76, and 77 were also examined. A conserved R158 was used as an internal control for validation of our analyses. All residue counts were normalized to the total number of amino acid occurrences (including gaps). Covariance analysis was performed to derive the evolutionary coupling (EC) information using EVfold server,[46,47] using the primary sequence of *E. coli* PagP (Uniprot ID P37001) as the template. ECs were scored using the pseudolikelihood maximization approach, and the default parameters were retained for the analysis. Information regarding the known residue contacts was obtained from the crystal structure of *E. coli* PagP (PDB ID 1THQ).

RESULTS

Enzymatic *in Vitro* Lipase Activity of PagP-St Is 15−20-Fold Higher than PagP-Ec Despite High Sequence and Structural Homology. The OM PagP barrel is present in certain pathogenic Gram-negative bacteria and displays a multitude of conserved residues, particularly the key catalytic triad amino acids that constitute the active site.[10] Our modeled structure of the *S. typhimurium* PagP (PagP-St) provides a global heavy atom root mean square deviation (RMSD) of 4.4 ± 2.9 Å against the *E. coli* PagP (PagP-Ec) crystal structure (Figure 1A). These values suggest that a high degree of structural, functional, and behavioral similarity is anticipated for the two PagP variants, owing to their high sequence conservation (Figure 1B). Pairwise alignment of both the PagP-St and PagP-Ec wild-type sequences points to six major differences in amino acids in the transmembrane region of the barrel (highlighted in Figure 1B) and to residue variations in the N-terminal helix. Not surprisingly, therefore, our results from MD simulations of both proteins in micellar systems do not highlight considerable differences in the *in silico* behavior of PagP-Ec and PagP-St (Figure 2). However, structural differences in the asymmetric *in vivo* membrane environment may be poorly captured in the simulation and cannot, therefore, be excluded.

To experimentally assess biochemical features of both proteins, and to probe the possible influence of six positional variations in the transmembrane domain (highlighted in Figure 1B), we refolded PagP-Ec and PagP-St in the *di*$C_{12:0}$PC 1,2-dilauroyl-*sn*-glycero-3-phosphocholine (DLPC) vesicles and in the $C_{12:0}$PC *n*-dodecylphosphocholine (DPC) micelles. Formation of well-folded β-barrel structures in both proteins is evident from local and global analyses using gel mobility shifts and spectroscopic measurements (Figure 3A−C). Indeed, it has been shown that several amphipols, detergents, and lipids support PagP structure.[10,15,22,23,40,44,48−50] To investigate the enzymatic activity, we assayed the catalytic ability colorimetrically by monitoring the rate of *p*-nitrophenol release from the

DOI: 10.1021/acs.biochem.5b00543
Biochemistry 2015, 54, 5712−5722

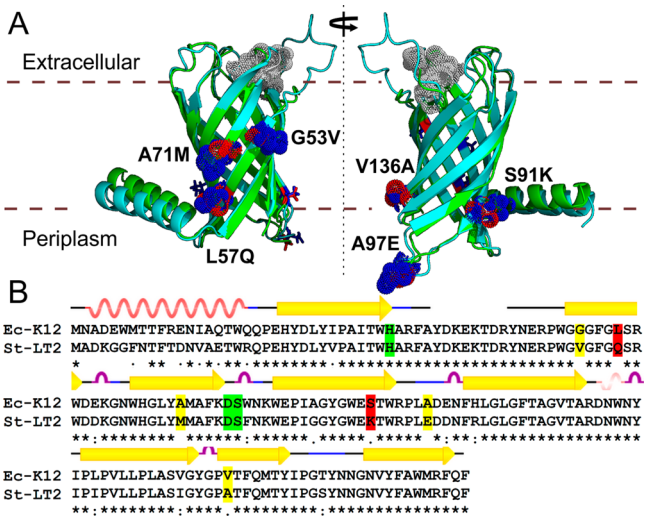

Figure 1. PagP barrel. (A) Superposition of the I-TASSER[59] generated PagP-St structure (cyan) on the crystal structure of PagP-Ec (green, PDB ID 3GP6[22]). The six residues in the transmembrane region that are noticeably different in both proteins (highlighted in the alignment in B) are rendered as surface dots (red (PagP-Ec) and blue (PagP-St)) and labeled (format: Ec residue, residue number, St residue). The three catalysis site residues are rendered in gray. (B) ClustalW[60] alignment of full-length PagP protein sequences from *E. coli* K12 (Ec-K12) and *S. typhimurium* LT2 (St-LT2). Catalytic site residues (the HDS triad) are highlighted in green, while the six differences are in red and yellow. Red highlights correspond to the mutants described in this study.

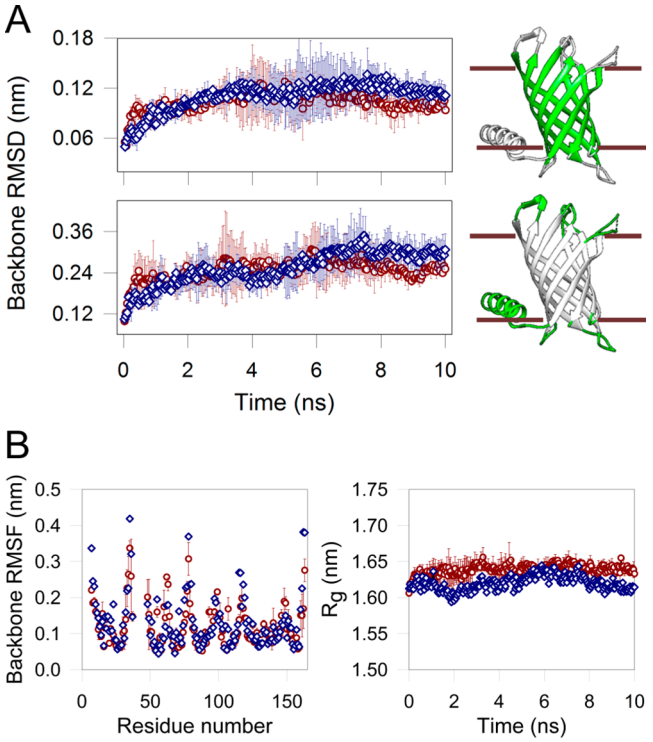

Figure 2. MD simulation studies of PagP in DPC micelles. (A) Averaged results from two independent 10 ns simulations of PagP-Ec (1THQ[20]) (red, circles) and PagP-St (generated by modification of 1THQ using CHARMM-GUI input generator) (blue, diamonds) structures, in 80 molecules of *n*-dodecylphosphocholine (DPC) micelles. Backbone RMSDs calculated for the transmembrane residues (top panel) and the extra-membrane residues (bottom panel) are similar for both proteins. The protein segments used for the RMSD calculation are shown as green in the cartoon provided on the right. (B, left) Residue-wise backbone root mean square fluctuations (RMSFs) averaged over the 10 ns simulation time show lower values for residues corresponding to the transmembrane region of the protein and a sharp rise in fluctuations for residues present in the loop regions. (B, right) Radius of gyration (R_g) values calculated for both proteins show that the barrel is stable throughout the simulation and that there is no discernible difference in the structural scaffold of both these proteins. The color/symbol codes described in (A) are retained in (B).

lipase substrate *p*NPP, as reported earlier.[25,51] The specific activity of 0.058 (±0.007) nmol/min/μM we obtain for PagP-Ec, although 3-fold slower than the natural phospholipid−lipid A substrates (compare Bishop et al., 2000[52] versus Huysmans et al., 2007[25]), is in good agreement with previous reports.[25,51] While there is considerable variation in the N-terminal helix residues for both proteins (Figure 1B), we have observed that the helix does not influence the catalytic properties (unpublished results), in line with previous studies.[25,29,53]

Unexpectedly, under identical assay conditions in various lipids (DLPC, DMPC, DPPC, DSPC, and *E. coli* total lipid extract), we observe a nearly 15-fold increase in PagP-St specific activity, compared to its structurally similar *E. coli* homologue (Figure 3D−F). The difference is translated into micellar systems, wherein we obtain values of 0.019 (±0.002) and 0.427 (±0.033) nmol/min/μM for PagP-Ec and PagP-St, respectively; we, therefore, find a 20-fold difference in activity in DPC. Note, however, that the activity is reduced by ∼3-fold in DPC pH 9.5 (versus DLPC pH 8.0) for both proteins. However, our measured *p*NPP hydrolysis rates are comparable in pH 8.0 (DPC), pH 9.5 (DPC) and pH 9.5 (*n*-dodecyl-β-D-maltopyranoside[54]) (data not shown). Considering that the active site residues, as well as those lining the substrate-binding regions are identical in both proteins, we construed that alterations in overall protein stability might give rise to the observed differences in lipase activity.

PagP Protein Stability Correlates Inversely with Activity: PagP-Ec Equilibrium Free Energy Is 2-Fold Higher. In our experiments, we can successfully unfold and refold PagP in DPC using GdnHCl, without any hysteresis (Supporting Information Figure S1).[44,55] Further, this allows us to monitor the folding process non-invasively, using changes in fluorescence of the naturally occurring indole side chain of tryptophan. PagP-Ec and PagP-St harbor 12 and 10 indoles, respectively; refolded PagP shows a $\lambda_{em\text{-}max}$ of 342 nm. Upon increasing the denaturant (GdnHCl) concentration, both proteins show reduction in Trp fluorescence intensity, accompanied by a prominent red shift in the $\lambda_{em\text{-}max}$ to >360 nm (Figure 4A). This change results from the GdnHCl solvation-mediated increase in polarity of the indole environment, as PagP unfolds.

We monitored the unfolding of both PagP-Ec and PagP-St at 342 nm, and fitted the data to a two-state linear unfolding model to obtain the extrapolated equilibrium free energy at zero denaturant (ΔG^0_U). We obtain ΔG^0_U values of −10.51 (±0.47) kcal/mol (PagP-Ec) and −6.46 (±0.28) kcal/mol (PagP-St), with the C_m values (midpoint of chemical denaturation) as −3.45 (±0.15) M and −2.83 (±0.11) M, for PagP-Ec and PagP-St, respectively (Figure 4B first panel, Table 1). While we observe a change in the unfolding cooperativity of both proteins (compare *m* values in Table 1), we deduce from the considerable differences in C_m that the stability of PagP-Ec results from the ability of this refolded protein to resist

DOI: 10.1021/acs.biochem.5b00543
Biochemistry 2015, 54, 5712−5722

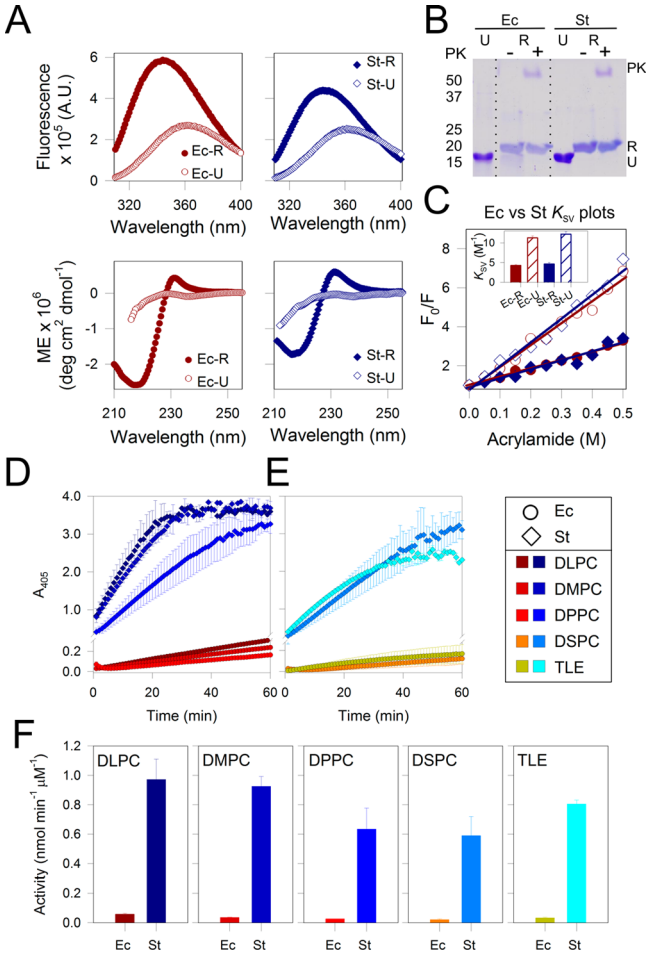

Figure 3. PagP refolding probed by spectroscopy and activity measurements. (A) Tryptophan emission spectra (top panels) and far-UV CD spectra (bottom panels) of PagP-Ec (Ec, red circles, left panels) and PagP-St (St, blue diamonds, right panels) refolded (R, filled symbols) in 10 mM DPC or unfolded (U, open symbols) using 8.0 M urea. Note the positive couplet at 231 nm, arising from stereospecific interaction of Y26 and W66 in refolded PagP. See text for details. A.U.: arbitrary units; ME: molar ellipticity. (B) Refolded (R) PagP-Ec and PagP-St display retarded gel mobility in SDS-PAGE and protection from digestion by proteinase K (PK), compared to the urea-unfolded (U) protein. Dotted lines separate different gel segments that are presented together. (C) Collisional quenching of Trp fluorescence using acrylamide demarcates folded (filled symbols) and unfolded (open symbols) proteins. Stern–Volmer constants (K_{SV}, inset) are considerably lower for the refolded protein, due to shielding of indole from the quencher. (D, E) Assay of PagP catalytic activity using 1 mM *p*NPP. Increase in A_{405} as *p*NPP is hydrolyzed to release *p*-nitrophenol is measured with time for 1.0 μM protein refolded in 1.2 mM lipid to derive the specific enzyme turnover (F). Note how the activity of PagP-St is >15-fold greater than PagP-Ec. In all panels, the PagP-Ec data are shown in shades of red (circles) and PagP-St in shades of blue (diamonds). Assay of PagP activity in DLPC, DMPC, and DPPC are shown in (D), while DSPC and total lipid extract (TLE) are provided in (E). Color codes for the various lipids are also indicated.

solvation by GdnHCl. This stability may result from augmented protein–micelle interaction strengths. We also note here that the difference between previously reported free energy values for PagP-Ec,[44,55] and our observed result can be attributed to the difference in protein–lipid interactions in vesicular systems versus micellar systems.

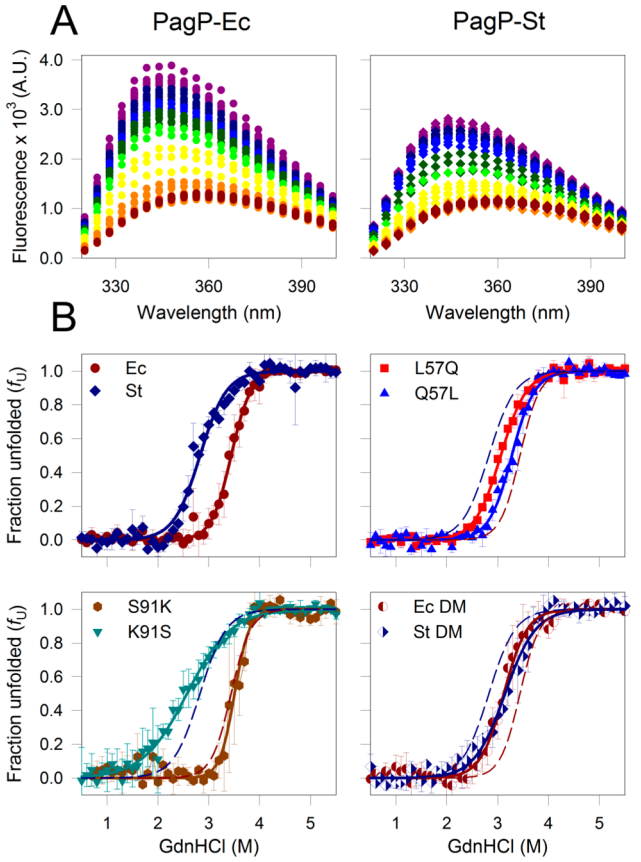

Figure 4. Equilibrium two-state transitions of PagP in GdnHCl. (A) Representative fluorescence emission scans of native PagP-Ec (left) and PagP-St (right) from low (purple) to high (red) denaturant, acquired after 24 h incubation in GdnHCl at 25 °C. A.U.: arbitrary units. (B) Unfolded protein fractions (f_U) calculated at the $\lambda_{em\text{-}max}$ of 342 nm for all the PagP variants described in this study. Data points have been averaged over at least three independent experiments and fitted to a two-state equation (fits are shown as solid lines). The unfolding profiles of native PagP-Ec and PagP-St are included as dashed lines in the data for the mutants. PagP-Ec (Ec): dark red, circles; PagP-St (St): dark blue, diamonds; PagP-Ec:L57Q (L57Q): red, squares; PagP-St:Q57L (Q57L): blue, upward triangles; PagP-Ec:S91K (S91K): brown, hexagons; PagP-St:K91S (K91S): dark cyan, downward triangles; PagP-Ec:DM (DM): dark red, semi-filled circles; PagP-St:DM (DM): dark blue, semi-filled diamonds.

Our results indicate that a quantifiable difference between both proteins (both in terms of catalytic efficiency and stability) is likely to arise from key variations between the protein sequences. There are six positional differences in the transmembrane region of PagP-Ec and PagP-St (see Figure 1B). Of particular interest are positions 57 and 91, where there is a significant change in the chemical nature of the residue. Notably, our calculated energetic costs for substitutions at these positions, based on previous findings,[56] are 2–4 fold higher than the other variations (shown in Supporting Information Figure S2). Hence, we mapped the contributions of these residues to the global protein stability as well as their influence on the catalytic activity, by generating site-specific mutants.

Single-Residue Substitutions Considerably Affect Thermodynamic Stability but Are Non-Additive Across PagP Variants. We achieve comparable folding efficiency and β-rich structure in DPC for the two single mutants (*E. coli* PagP mutants: PagP-Ec:L57Q and PagP-Ec:S91K; *S. typhimurium*

DOI: 10.1021/acs.biochem.5b00543
Biochemistry 2015, 54, 5712–5722

Table 1. Thermodynamic Parameters for PagP Derived from Equilibrium Chemical Denaturation

	PagP-Ec				PagP-St			
protein	ΔG^0_U (kcal mol^{-1})	m (kcal mol^{-1} M^{-1})	C_m (M)	$C_{m\text{-}r}$ (M)	ΔG^0_U (kcal mol^{-1})	m (kcal mol^{-1} M^{-1})	C_m (M)	$C_{m\text{-}r}$ (M)
Ec < > St	10.51 ± 0.47	−3.05 ± 0.14	3.45 ± 0.15	3.56 ± 0.03	6.46 ± 0.28	−2.28 ± 0.09	2.83 ± 0.11	3.04 ± 0.02
L57Q < > Q57L	7.12 ± 0.20	−2.33 ± 0.06	3.06 ± 0.09	2.98 ± 0.04	8.61 ± 0.38	−2.63 ± 0.11	3.28 ± 0.14	3.39 ± 0.03
S91K < > K91S	13.70 ± 1.17	−3.89 ± 0.33	3.53 ± 0.29	3.39 ± 0.03	3.01 ± 0.15	−1.16 ± 0.06	2.59 ± 0.13	2.84 ± 0.02
DM[a]	8.01 ± 0.46	−2.57 ± 0.15	3.12 ± 0.18	3.12 ± 0.03	6.51 ± 0.28	−2.06 ± 0.09	3.16 ± 0.14	3.47 ± 0.02

[a]Double mutants, namely, PagP-Ec:L57Q+S91K and PagP-St:Q57L+K91S.

mutants: PagP-St:Q57L and PagP-St:K91S) and the double mutants (PagP-Ec:DM, bearing L57Q and S91K; PagP-St:DM, bearing Q57L and K91S) (see sequence alignment in Figure 1B; Supporting Information Figure S3). Data from single-residue substitutions at position 57 clearly reveal that Leu confers an added ∼2.2 kcal/mol stabilization to native PagP-St (Figure 4B and Table 1), which is anticipated from burial of the apolar Leu in the micelle core; the corresponding burial of Gln destabilizes PagP-Ec by ∼3.5 kcal/mol. The overall barrel stability is affected by concurrent variations in both the unfolding cooperativity (m value) and denaturant solvation effects (C_m) (Table 1).

Contrary to the expected stabilization of ∼3.56 kcal/mol (see Supporting Information Figure S2), the PagP-St:K91S barrel shows a diametrically opposite result, with a 2-fold reduction in the protein stability (by ∼3.45 kcal/mol). PagP-Ec:S91K, on the other hand, is stabilized by ∼3.0 kcal/mol, in comparison with the parent protein. Interestingly, in both cases, the change in free energy arises predominantly from contribution of the m value, which is higher for PagP-Ec:S91K. Hence, this mutation causes burying of a greater surface area in PagP-Ec:S91K protein, compared to the other constructs studied herein, raising the m value closer to those obtained for PagP in phosphocholine large unilamellar vesicles,[44,55] without considerable changes in the secondary structure of the protein (data not shown).

Double mutants of both barrels at positions 57 and 91 display a non-additive effect on the overall thermodynamic parameters (Figure 4B and Table 1). Recovery of the ΔG^0_U for PagP-St:DM is afforded primarily by L57, which offsets the destabilization of S91. However, the overwhelming stability due to K91 in PagP-Ec is insufficient to counteract the destabilization arising as a consequence of Q57. We observe only a marginal increase of ∼0.25 kcal/mol in the m value of PagP-Ec:DM over PagP-Ec:L57Q, as a result of which the overall protein stability of the double mutant is lower than wild-type PagP-Ec.

Global Differences in Biophysical Parameters Retained Across Mutants Bear No Subjective Evidence to the Activity of This Outer Membrane Enzyme. We monitored the biophysical properties of PagP and its mutants by measuring fluorescence lifetime and anisotropy (Supporting Information Figure S4 and Supporting Information Table S2). The midpoint of chemical denaturation from anisotropy measurements ($C_{m\text{-}r}$), for example, follows a similar GdnHCl-dependence as the fluorescence intensities, although all $C_{m\text{-}r}$ values are higher than the corresponding C_m values by ∼0.2 M. GdnHCl-solvation of Trp, therefore, precedes unfolding process in PagP, and is not affected by the mutations. Further, $\langle\tau\rangle$, K_{SV}, and bimolecular quenching constant (k_q) are similar (Supporting Information Table S2). These data indicate that global differences across the PagP mutants and their biophysical properties are conserved.

Contrastingly, the differences in biophysical properties of PagP-Ec, PagP-St, and the site-specific mutants are not reflected in their enzymatic turnover (Figure 5). For instance, in PagP-St,

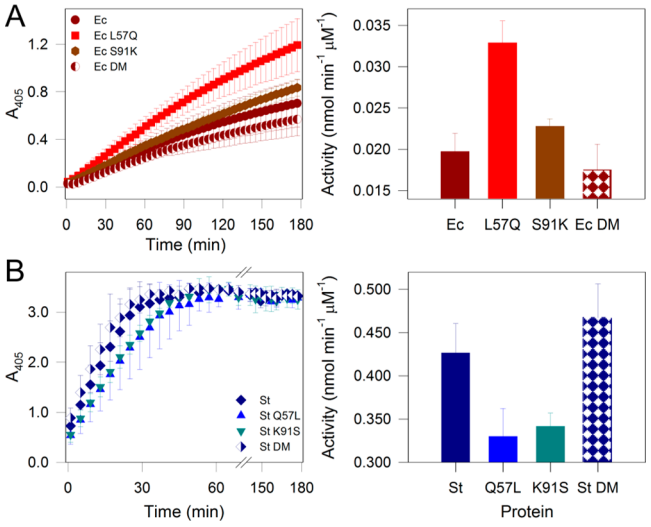

Figure 5. Assay of PagP catalytic activity in DPC micelles using 1 mM *p*NPP as the substrate analogue. Change in A_{405} (absorbance at 405 nm) as an indicator of *p*NPP hydrolysis and *p*-nitrophenol release. Data obtained using 2.0 μM protein refolded in 10 mM DPC are averaged over three independent experiments and shown on the left (A, Ec proteins; B, St proteins). Specific enzyme turnover for the various constructs are summarized as histograms on the right. Color/symbol schemes are similar to Figure 4.

the single mutants PagP-St:Q57L and PagP-St:K91S are the most and least thermodynamically stable variants, respectively (see Table 1); however, both proteins exhibit comparable (and poor) activity (Figure 5, lower panels). Similarly, in the case of PagP-Ec, protein stability follows the rank order S91K > WT > DM > L57Q (Table 1), while the activity assay gives us the rank order L57Q > S91K > WT > DM (Figure 5). Our calculated values for free energy and *p*NPP hydrolysis are derived in DPC micelles and may differ from PagP refolded in vesicles[44,55] or when palmitoyltransfer is monitored.[30] However, we believe that the rank order we obtain for both stability and activity might translate well to the native lipidic environment of the bacterial outer membrane.

We neither observe an additive effect of the mutations on the folding free energy nor the protein activity. Furthermore, while the PagP-Ec:L57Q and PagP-St:Q57L stabilities differ only by ∼1.5 kcal/mol, a 10-fold difference in their activity is apparent, with PagP-St being higher. Hence, what we obtain is an ostensible paradox in correlations between the structural and

DOI: 10.1021/acs.biochem.5b00543
Biochemistry 2015, 54, 5712−5722

functional properties of PagP from *E. coli* and *S. typhimurium*, despite their unusually high sequence identity. In our attempts to identify underlying elements within the chemical nature of these residues that simultaneously show a pronounced influence on these seemingly unrelated structural and enzymatic features of the barrels, we examined the thermostability of all PagP variants.

PagP Exhibits Thermostability in DPC but Variations in Tertiary Interactions Are Conserved Across Mutants. Previous reports have exemplified the unusual stability of PagP to denaturation at very high temperatures, in the absence of chemical denaturants such as SDS or urea.[25] However, unfolding of the protein refolded in lauryldimethylamine oxide (another 12-C detergent similar to DPC) has been observed at temperatures beyond 80 °C.[26] In DPC, we find a reversible ∼30−40% loss in the secondary structure of the PagP barrel variants at the highest experimentally achievable temperature of 95 °C (Figure 6A,B; also see Supporting Information Figure S5). Hence, quantitative conclusions cannot be achieved using the 215 nm data for the β-sheet structure, in DPC.

In addition to the signature negative maximum at 215 nm, correctly folded PagP also exhibits a characteristic tertiary CD Cotton effect with an observable positive maximum at ∼231 nm,[26,54] and a negative maximum at ∼225 nm (masked by the backbone contribution) (Figure 6A). The exciton couplet emanates from stereospecific orientation of Y26 and W66 (numbering from PagP-Ec[26]). We therefore gauged the influence of mutations on the temperature-dependent loss of the interacting aryl dipoles (Figure 6B; also see Supporting Information Figure S5), as an indicator of the overall scaffold stability, by defining the $T_{m\text{-start}}$ temperature.[45] This temperature is the point where unfolding commences (or the point of recovery from thermal denaturation) and can be determined confidently for PagP variants lacking a two-state unfolding baseline.

Figure 6C summarizes the $T_{m\text{-start}}$ for the unfolding and refolding arms of the thermal profiles monitored at 231 nm and provides us with interesting facets of PagP behavior. The occurrence of hysteresis is evident by the ∼5−10% difference between the unfolding and recovery $T_{m\text{-start}}$ values, with the latter being lower. A corresponding difference in the secondary structure is not seen (Figure 6A, insets and top panels of 6B), indicating that robustness of the Y26/W66 interaction depends on integrity of the barrel structure. The latter, in turn, is determined by interaction strengths of residues lining the barrel exterior with the hydrocarbon tail of DPC. Furthermore, reassembly of the PagP barrel with DPC involves two reactants (protein and micelle), whereas unfolding occurs for a unified protein-micelle body. Refolding is therefore completed at lower temperatures wherein the relative Brownian motion is concurrently reduced. This difference also accounts for the observed hysteresis in our thermal denaturation measurements. A similar observation has been reported for *E. coli* OmpX.[45]

The $T_{m\text{-start}}$ of PagP-Ec is 86 (±2.26) °C, whereas unfolding of PagP-St is initiated at 78 (±0.21) °C. The stability pattern observed in the respective PagP mutants from GdnHCl denaturation (see Figure 4B and Table 1) is also faithfully reproduced in the $T_{m\text{-start}}$ values. Yet, the magnitude of difference observed does not correlate directly across PagP-Ec and PagP-St. For instance, PagP-St:Q57L and PagP-Ec:S91K are the most stable barrel variants for *Salmonella* and *Escherichia* PagP proteins, respectively. However, the equilibrium free

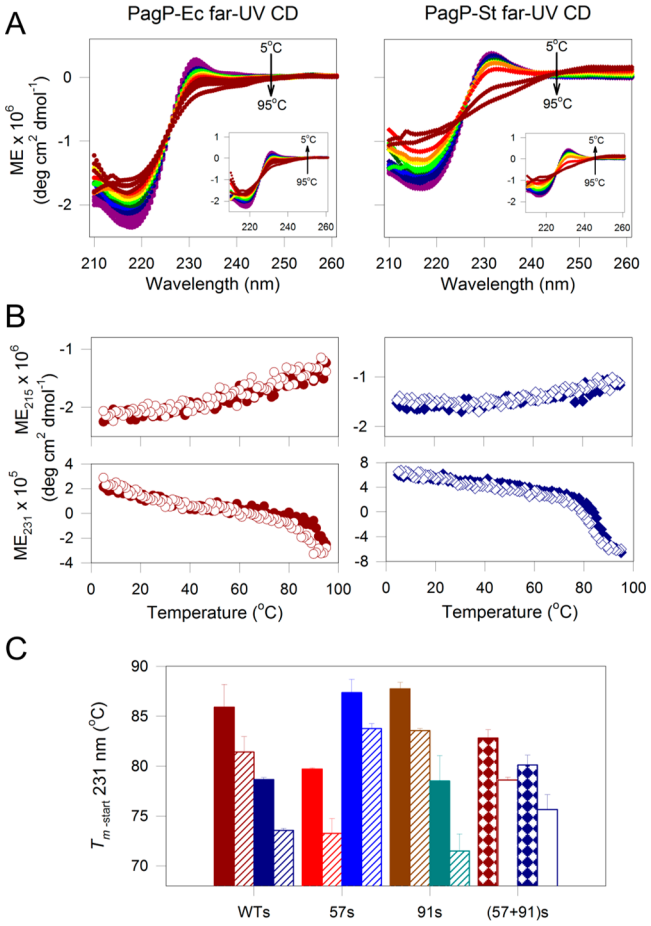

Figure 6. Response of PagP to thermal denaturation. (A) Representative far-UV CD wavelength scans of PagP-Ec (left) and PagP-St (right) undergoing thermal denaturation when heated from 5 °C (purple) → 95 °C (red) and recovery (insets) profiles recorded from 95 °C → 5 °C. Spectra were recorded at increments of 10 °C. ME: molar ellipticity. (B) Unfolding (filled symbols) and refolding (open symbols) response of PagP-Ec (left, red circles) and PagP-St (right, blue diamonds) monitored at 215 nm (molar ellipticity at 215 nm, ME_{215}) for β-sheet content or ME_{231} for changes in the exciton contribution. The loss in β-sheet structure is largely linear and changes by only ∼30%, suggesting incomplete protein unfolding within the experimental temperature range. The ME_{231} shows a sigmoidal profile, with unfolding initiated beyond ∼80−90 °C for both proteins. (C) Comparison of $T_{m\text{-start}}$ values derived for the CD thermal denaturation curves at 231 nm for the unfolding (filled or patterned histograms) and recovery (striped or unfilled histograms) for wild-type PagP (WTs), mutation at position 57 (57s) or 91 (91s) or double mutants ((57 + 91)s). Error bars represent standard deviations derived from two independent data sets. Color schemes are retained from Figure 4.

energy values differ by ∼5.5 kcal/mol, whereas the $T_{m\text{-start}}$ values are nearly identical (∼87 °C and ∼83 °C for the unfolding and refolding profiles, respectively). Similar differences are observed for the other PagP mutants and suggest that guanidine solvation effects unfold PagP scaffold through different mechanisms, compared to perturbation by temperature.

Key Residue Contributions Correlate with Sequence Variation and β-Barrel Scaffold Plasticity, Matching Stability with Catalysis. Our data provide us with unique features of PagP that emerge from interlinking barrel structure, catalytic proficiency, and the overall stability. It has not escaped

DOI: 10.1021/acs.biochem.5b00543
Biochemistry 2015, 54, 5712−5722

our notice that the unusual structural features of PagP (25° barrel tilt and the N-terminal helix) distinguish this protein from other OM 8-stranded β-barrels.[20,22] We, therefore, examined whether biological manifestations of the observed evolutionary choices in amino acids could exist for this barrel. For this, we surveyed for conservation patterns in the chemical nature of PagP residues across known PagP sequences from bacteria that are pathogenic and nonpathogenic to humans (Supporting Information Figure S6). This analysis may bear relevance to the efficacy of lipid A mediated immune response,[6,7,17,30] decided by the activity of PagP. It must be noted here that the transmembrane domains of *S. typhimurium* and *S. typhi* share identical PagP sequences (G5/W5 and H22/Y22 are the only sites with differences between *S. typhimurium* and *S. typhi*). However, we did not consider whether the PagP is functional in the host bacterium, for this analysis.

At position 57, Leu is equally abundant in all bacterial types; on the other hand, PagP-St harbors the less abundant Gln, instead of Lys, which is frequented in pathogens. Evidently, the evolutionary selection of Q57 in *Salmonella* might therefore not relate to its pathogenicity. Indeed, examination of our biophysical and biochemical analyses suggests that while the refolded PagP-St:Q57L is more stable, it displays the poorest catalytic ability of all the PagP-St variants (see Figure 5). Similarly, replacement of L57 in PagP-Ec (the PagP-Ec:L57Q mutant) enhances catalysis 1.5-fold at the expense of considerable protein destabilization (~3.5 kcal/mol).

At position 91, we obtain a preponderance of Lys in pathogenic and mildly pathogenic bacteria such as *S. typhi*, *Y. pestis*, *B. pertussis*, and *L. pneumophila* (Supporting Information Figure S6). However, *Y. pestis* and *B. pertussis* do not possess a functional *pagP* gene, while *Y. enterocolitica*, *Y. pseudotuberculosis*, and *B. bronchiseptica* have functional *pagP* genes.[13] Hence, it is not clear if this residue is important for the *in vivo* function of PagP and/or for pathogenesis. From our *in vitro* experiments, we note that the PagP-Ec:S91K displays enhanced stability and activity (compared to the parent PagP-Ec construct); lowering in catalytic rates and an ~3.5 kcal/mol loss in stability seen in PagP-St:K91S is commensurate with expected results. At this point, we speculate that concurrent mutations at 57 and 91 might have been eliminated evolutionarily to possibly balance the contribution of both residues to PagP functional requirements in the specific bacterium, protein stability, and the overall barrel plasticity.

We further carried out a covariance analysis[46,47] of PagP sequences and derived a contact map of evolutionary couplings (ECs) based on the *E. coli* PagP sequence (Uniprot ID P37001) and crystal structure (PDB ID 1THQ). The results are provided in Supporting Information Figure S7 and Table S3. Several of the top-ranked evolutionarily constrained residues of PagP (Supporting Information Table S3) were present in the N-terminal helical region, the role of which has been extensively characterized previously.[25] We have examined the role of the N-terminal helix in the stability and activity of both PagP-Ec and PagP-St, and we observe that the N-terminal helix does not significantly alter the catalytic properties of these two homologous barrels (unpublished results). The six positional differences in the transmembrane region that we have mapped between PagP-Ec and PagP-St are distributed across the top 40% of the evolutionarily constrained residue positions. Our experimental findings on the 91st positional mutants of PagP-Ec and PagP-St, coupled with the bioinformatics analysis using sequences from the PFAM database (Supporting Information Figure S6), point toward an important role for the chemical nature of the residue present in this position in PagP function and stability.

We summarize the structural and functional characteristics imparted by the 57th and 91st residues of PagP in Figure 7.

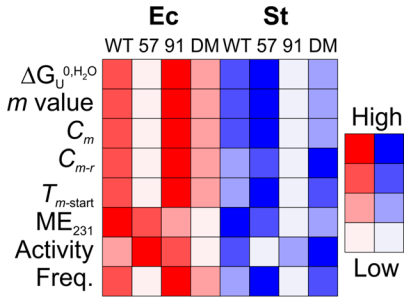

Figure 7. Comparison of biophysical, structural, and catalytic features of PagP. Native (WT) PagP-Ec and its mutants are shown in shades of red, while WT PagP-St and its mutants are depicted in shades of blue. Single mutants are indicated by their positions (for example, 57 corresponds to PagP-Ec:L57Q or PagP-St:Q57L), and the double mutant (57 + 91) is marked as DM. Note how in both bacteria, mutation at either site displays an overall inverse correlation between stability and enzymatic activity. "Freq " refers to the frequency of occurrence of the residue in pathogenic bacteria (refer to Supporting Information Figure S6).

This comparison brings out the global correlation between the superficially unrelated variations we obtain in the stability and activity of PagP. In the case of PagP-Ec, the single mutant PagP-Ec:S91K is the most stable and also shows considerable activity. The occurrence of Lys at position 91 in *E. coli* would, in general, be preferred over Ser if the bacterium required increased PagP specific activity. On the other hand, despite being highly active, PagP-Ec:L57Q has the lowest frequency of occurrence (lowest row in the left panel of Figure 7), probably because it is the least stable of all the PagP-Ec variants.

A similar inference can be drawn from the PagP-St summarized data (Figure 7, the right panel in shades of blue). In this case, PagP-St:Q57L is a mutant with high stability, but whether this organism compromised the stability of PagP for high enzymatic activity by selectively incorporating a Gln at position 57 requires further investigation. In both proteins, the double mutants display either a compromised stability or lower activity. Minor residue variations in a protein, which is otherwise ubiquitous in several Gram-negative bacteria, might therefore demarcate structurally similar β-barrel scaffolds on a scale of thermodynamic stability.

Our deductions relating the distal mutations with function or infectivity should be interpreted with a certain level of caution, since our bioinformatics analyses also disclose glaring exceptions to the rule. For instance, PagP-Ec belonging to the nonpathogenic strain (K12) is virtually identical in sequence to one belonging to the pathogenic strain (0157:H7) or to *Shigella* PagP.[29] Further, our assays of activity and stability are limited to micellar systems, which do not necessarily mimic the native state of the PagP barrel in the bacterial outer membrane. Whether subtle sequence variations that result in magnitudes of difference in thermodynamic and functional features can manifest itself during differentiation and speciation in bacteria, while remaining camouflaged in analyses of the primary or tertiary protein structure, would certainly constitute an intriguing area for exploration.

DOI: 10.1021/acs.biochem.5b00543
Biochemistry 2015, 54, 5712−5722

DISCUSSION

S. typhimurium PagP shares a near-identical primary protein sequence to its highly pathogenic homologue *S. typhi*—the human typhoid causing bacterium.[1−4,57] Both proteins differ only at two sites: the fifth residue situated in the N-terminal helix and the 22nd residue at the start of the first transmembrane strand (G5 → W and H22 → Y in *S. typhi*). Previous studies using *E. coli* PagP have identified specific residues in this protein, which are involved in determining substrate (donor) specificity and enzymatic activity.[10,20,22] However, these mutations do not affect the ability of PagP to refold and insert in the bacterial outer membrane, or the stability of the protein. Our studies highlight the consequence of mutating residues in the structured transmembrane region of the barrel, on PagP stability and catalysis. The data presented here from *S. typhimurium* PagP provides new insight on the relationship between seemingly insignificant distal mutations in amino acids with the measured stability and activity of this protein. Compensation for protein stability to increase dynamicity and facilitate reactivity is observed from our *in vitro* study of PagP, suggesting that proteins with nearly identical structure and function can show unanticipated behavioral differences. Our data provide considerable evidence that the site-specific mutations are non-additive. Hence, we are tempted to propose that stabilizing and destabilizing effects of residue substitutions in PagP might have undergone a non-contact based coevolution.

Even for proteins such as PagP of *E. coli* and *S. typhimurium*, which are nearly identical in sequence and structure, we observe interesting challenges in correlating the protein thermodynamic stability with its associated enzymatic abilities. The conservation of key catalytic residues (H33, D76, S77) across all known bacterial species has been established thus far. In the case of PagP, the main function of this protein is the palmitoylation of lipid A. Modification of lipid A is required for survival of bacteria under the stress imposed by the foreign host.[13,19] Hence, the important elements that affect the survival of the bacterium include (i) rate with which lipid A palmitoylation is carried out by PagP, determined by its catalytic ability;[16] (ii) the residence time of the protein in the bacterial outer membrane, which is contributed by the protein stability;[44,58] and (iii) the timed expression of this protein, which is controlled by the PhoPQ regulon.[7,8] Through this study, we show that perturbing residues that are considerably away from the active site can moderate the activity of PagP *in vitro* in micelles and lipid vesicles. Such mutations change the stability of PagP-Ec and PagP-St by up to 2-fold. This observed change in overall barrel plasticity (Figures 4 and 6), and its correlation to catalytic activity in lipid vesicles (Figure 5), indicates that in the case of membrane proteins, function and structure can be correlated. It would be interesting to study whether these differences translate to significant implications *in vivo* for *Salmonella*. We envision that PagP stability can facilitate tight regulation of its turnover number, and its brief residence time in the *Salmonella* OM[30] may be sufficient for PhoPQ-controlled modification of both phosphatidylglycerol and lipid A. It has indeed been observed that the *pagP* gene may be differentially regulated by the PhoPQ regulon in various bacteria.[14,30]

The lipid composition of bacterial outer membranes not only differs across various species[13,16,17] but is also subjected to alterations during host invasion.[17,28−30] Changes in lipid composition can influence the stability of a barrel such as PagP, which demonstrates considerable structural tilt with respect to the bilayer normal. Whether *Salmonella* regulates protein turnover by lowering the stability of PagP, a protein that otherwise displays high thermodynamic stability in *E. coli*,[44,51,55] through selected replacement of distal residues, would constitute a fascinating study. The structural plasticity of PagP-Ec has been examined extensively using NMR,[23] and a model for substrate diffusion has been derived from these measurements. In general, high structural rigidity may be associated with increased resistance to denaturation, and thereby, a high free energy value in equilibrium measurements. However, structural rigidity hampers ready diffusion of the substrate into the barrel active site, and low enzymatic activity is recorded. Comparison of the stability and activity of PagP-Ec, PagP-St, and the mutants suggests that a correlation can be derived for most cases. Hence, a model emerges wherein residues distal from the active site enhance the function of PagP by lowering the structural rigidity of the barrel. We note that K91 is retained in organisms such as *S. typhi* and *L. pneumophila*.[10,13] The mutation of this residue lowers the stability and catalytic activity of PagP-St in our study. Different bacteria could, therefore, have evolved with subtle sequence variations in their PagP gene, based on the selection pressure of their environment. We speculate at this point that mutations at distal residues could influence the catalytic efficiency of PagP, by facilitating substrate diffusion into the barrel hydrocarbon ruler.[20,23,24,27] Whether such distal mutations can have an influence on the specific site of lipid A palmitoylation is also unclear.

Through this study, we provide evidence for the structural plasticity and enzymatic proficiency, modulated by specific amino acid variations, in the transmembrane β-barrel protein PagP. Our findings suggest that a global correlation exists between the influences of amino acids distal from the active site, with the observed thermodynamic features. We also show that *Salmonella* PagP is enzymatically more robust than *E. coli* PagP when it is refolded in various lipid vesicles. The observation that subtle variations affect the malleability of an eight-stranded transmembrane β-barrel may be applicable to other systems. Activity-stability trade-offs are always interpreted with respect to active site residues—in our study, we demonstrate that distal residues play a crucial role. Selectively altered binding specificities and activity in membrane proteins *in vitro* and *in vivo*, using PagP as the model system, could help in understanding evolutionary differences in pathogen selection and survival, paving the way for customized drug targeting.

ASSOCIATED CONTENT

Supporting Information

The Supporting Information is available free of charge on the ACS Publications website at DOI: 10.1021/acs.biochem.5b00543.

Supporting figures and tables (PDF)

AUTHOR INFORMATION

Corresponding Author

*Address: Molecular Biophysics Laboratory, Department of Biological Sciences, Indian Institute of Science Education and Research, Transit campus: ITI Building, Govindpura, Bhopal 462023, India. Tel.: 91-755-4092318. Fax: 91-755-4092392. E-mail: maha@iiserb.ac.in.

DOI: 10.1021/acs.biochem.5b00543
Biochemistry 2015, 54, 5712−5722

Funding

This work was supported by the Department of Biotechnology Grants BT/HRD/35/02/25/2009, BT/01/IYBA/2009 from the Government of India to R.M.

Notes

The authors declare no competing financial interest.

■ ACKNOWLEDGMENTS

We gratefully acknowledge the anonymous reviewers for their insightful comments and suggestions. B.R.I acknowledges senior research fellowship from the University Grants Commission, Govt. of India. R.M. is a Wellcome Trust/DBT India Alliance Intermediate Fellow.

■ ABBREVIATIONS

CD, circular dichroism spectropolarimetry; C_m, midpoint of chemical denaturation or renaturation; DLPC, 1,2-dilauroyl-*sn*-glycero-3-phosphocholine; DPC, *n*-dodecylphosphocholine; DPR, detergent-to-protein ratio; LPR, lipid-to-protein ratio; GdnHCl, guanidine hydrochloride; K_{SV}, Stern−Volmer constant; k_q, bimolecular quenching constant; *m* value, unfolding cooperativity; MD, molecular dynamics; ME, molar ellipticity; OM, outer membrane; PagP, PhoP/PhoQ-activated gene P; PagP-Ec, full-length mature PagP protein without the signal peptide, from *E. coli*; PagP-St, full-length mature PagP protein without the signal peptide, from *S. typhimurium*; PC, phosphatidylcholine; *r*, anisotropy value; TM, transmembrane; ΔG^0_U, equilibrium unfolding free energy; $\lambda_{ex\text{-}max}$, fluorescence excitation maximum; *p*NPP, *p*-nitrophenyl palmitate; $\langle\tau\rangle$, average lifetime

■ REFERENCES

(1) Haraga, A., Ohlson, M. B., and Miller, S. I. (2008) Salmonellae interplay with host cells. *Nat. Rev. Microbiol. 6*, 53−66.

(2) de Jong, H. K., Parry, C. M., van der Poll, T., and Wiersinga, W. J. (2012) Host-pathogen interaction in invasive Salmonellosis. *PLoS Pathog. 8*, e1002933.

(3) Dougan, G., and Baker, S. (2014) *Salmonella enterica* serovar *Typhi* and the pathogenesis of typhoid fever. *Annu. Rev. Microbiol. 68*, 317−336.

(4) Wain, J., Hendriksen, R. S., Mikoleit, M. L., Keddy, K. H., and Ochiai, R. L. (2015) Typhoid fever. *Lancet 385*, 1136−1145.

(5) http://www.cdc.gov/nczved/divisions/dfbmd/diseases/typhoid_fever/technical.html and http://www.cdc.gov/salmonella/.

(6) Guo, L., Lim, K. B., Poduje, C. M., Daniel, M., Gunn, J. S., Hackett, M., and Miller, S. I. (1998) Lipid A acylation and bacterial resistance against vertebrate antimicrobial peptides. *Cell 95*, 189−198.

(7) Murata, T., Tseng, W., Guina, T., Miller, S. I., and Nikaido, H. (2007) PhoPQ-mediated regulation produces a more robust permeability barrier in the outer membrane of *Salmonella enterica* serovar *typhimurium*. *J. Bacteriol. 189*, 7213−7222.

(8) Prost, L. R., and Miller, S. I. (2008) The Salmonellae PhoQ sensor: mechanisms of detection of phagosome signals. *Cell. Microbiol. 10*, 576−582.

(9) Robey, M., O'Connell, W., and Cianciotto, N. P. (2001) Identification of *Legionella pneumophila* rcp, a pagP-like gene that confers resistance to cationic antimicrobial peptides and promotes intracellular infection. *Infect. Immun. 69*, 4276−4286.

(10) Hwang, P. M., Choy, W. Y., Lo, E. I., Chen, L., Forman-Kay, J. D., Raetz, C. R., Prive, G. G., Bishop, R. E., and Kay, L. E. (2002) Solution structure and dynamics of the outer membrane enzyme PagP by NMR. *Proc. Natl. Acad. Sci. U. S. A. 99*, 13560−13565.

(11) Preston, A., Maxim, E., Toland, E., Pishko, E. J., Harvill, E. T., Caroff, M., and Maskell, D. J. (2003) Bordetella bronchiseptica PagP is a Bvg-regulated lipid A palmitoyl transferase that is required for persistent colonization of the mouse respiratory tract. *Mol. Microbiol. 48*, 725−736.

(12) Pilione, M. R., Pishko, E. J., Preston, A., Maskell, D. J., and Harvill, E. T. (2004) pagP is required for resistance to antibody-mediated complement lysis during Bordetella bronchiseptica respiratory infection. *Infect. Immun. 72*, 2837−2842.

(13) Bishop, R. E., Kim, S. H., and El Zoeiby, A. (2005) Role of lipid A palmitoylation in bacterial pathogenesis. *J. Endotoxin Res. 11*, 174−180.

(14) Monsieurs, P., De Keersmaecker, S., Navarre, W. W., Bader, M. W., De Smet, F., McClelland, M., Fang, F. C., De Moor, B., Vanderleyden, J., and Marchal, K. (2005) Comparison of the PhoPQ regulon in *Escherichia coli* and *Salmonella typhimurium*. *J. Mol. Evol. 60*, 462−474.

(15) Kleinschmidt, J. H. (2015) Folding of *β*-barrel membrane proteins in lipid bilayers − unassisted and assisted folding and insertion. *Biochim. Biophys. Acta, Biomembr. 1848*, 1927−1943.

(16) Whitfield, C., and Trent, M. S. (2014) Biosynthesis and export of bacterial lipopolysaccharides. *Annu. Rev. Biochem. 83*, 99−128.

(17) Needham, B. D., and Trent, M. S. (2013) Fortifying the barrier: the impact of lipid A remodelling on bacterial pathogenesis. *Nat. Rev. Microbiol. 11*, 467−481.

(18) Ernst, R. K., Yi, E. C., Guo, L., Lim, K. B., Burns, J. L., Hackett, M., and Miller, S. I. (1999) Specific lipopolysaccharide found in cystic fibrosis airway *Pseudomonas aeruginosa*. *Science 286*, 1561−1565.

(19) Khan, S. A., Everest, P., Servos, S., Foxwell, N., Zahringer, U., Brade, H., Rietschel, E. T., Dougan, G., Charles, I. G., and Maskell, D. J. (1998) A lethal role for lipid A in *Salmonella* infections. *Mol. Microbiol. 29*, 571−579.

(20) Ahn, V. E., Lo, E. I., Engel, C. K., Chen, L., Hwang, P. M., Kay, L. E., Bishop, R. E., and Prive, G. G. (2004) A hydrocarbon ruler measures palmitate in the enzymatic acylation of endotoxin. *EMBO J. 23*, 2931−2941.

(21) Evanics, F., Hwang, P. M., Cheng, Y., Kay, L. E., and Prosser, R. S. (2006) Topology of an outer-membrane enzyme: Measuring oxygen and water contacts in solution NMR studies of PagP. *J. Am. Chem. Soc. 128*, 8256−8264.

(22) Cuesta-Seijo, J. A., Neale, C., Khan, M. A., Moktar, J., Tran, C. D., Bishop, R. E., Pomes, R., and Prive, G. G. (2010) PagP crystallized from SDS/cosolvent reveals the route for phospholipid access to the hydrocarbon ruler. *Structure 18*, 1210−1219.

(23) Hwang, P. M., Bishop, R. E., and Kay, L. E. (2004) The integral membrane enzyme PagP alternates between two dynamically distinct states. *Proc. Natl. Acad. Sci. U. S. A. 101*, 9618−9623.

(24) Khan, M. A., and Bishop, R. E. (2009) Molecular mechanism for lateral lipid diffusion between the outer membrane external leaflet and a beta-barrel hydrocarbon ruler. *Biochemistry 48*, 9745−9756.

(25) Huysmans, G. H., Radford, S. E., Brockwell, D. J., and Baldwin, S. A. (2007) The N-terminal helix is a post-assembly clamp in the bacterial outer membrane protein PagP. *J. Mol. Biol. 373*, 529−540.

(26) Khan, M. A., Neale, C., Michaux, C., Pomes, R., Prive, G. G., Woody, R. W., and Bishop, R. E. (2007) Gauging a hydrocarbon ruler by an intrinsic exciton probe. *Biochemistry 46*, 4565−4579.

(27) Khan, M. A., Moktar, J., Mott, P. J., Vu, M., McKie, A. H., Pinter, T., Hof, F., and Bishop, R. E. (2010) Inscribing the perimeter of the PagP hydrocarbon ruler by site-specific chemical alkylation. *Biochemistry 49*, 9046−9057.

(28) Solnick, J. V., Hansen, L. M., Salama, N. R., Boonjakuakul, J. K., and Syvanen, M. (2004) Modification of *Helicobacter pylori* outer membrane protein expression during experimental infection of rhesus macaques. *Proc. Natl. Acad. Sci. U. S. A. 101*, 2106−2111.

(29) Smith, A. E., Kim, S. H., Liu, F., Jia, W., Vinogradov, E., Gyles, C. L., and Bishop, R. E. (2008) PagP activation in the outer membrane triggers R3 core oligosaccharide truncation in the cytoplasm of *Escherichia coli* O157:H7. *J. Biol. Chem. 283*, 4332−4343.

(30) Dalebroux, Z. D., Matamouros, S., Whittington, D., Bishop, R. E., and Miller, S. I. (2014) PhoPQ regulates acidic glycerophospholipid content of the *Salmonella Typhimurium* outer membrane. *Proc. Natl. Acad. Sci. U. S. A. 111*, 1963−1968.

DOI: 10.1021/acs.biochem.5b00543
Biochemistry 2015, 54, 5712−5722

(31) Van Der Spoel, D., Lindahl, E., Hess, B., Groenhof, G., Mark, A. E., and Berendsen, H. J. (2005) GROMACS: fast, flexible, and free. *J. Comput. Chem. 26*, 1701−1718.
(32) Cox, K., and Sansom, M. S. (2009) One membrane protein, two structures and six environments: a comparative molecular dynamics simulation study of the bacterial outer membrane protein PagP. *Mol. Membr. Biol. 26*, 205−214.
(33) Lomize, M. A., Lomize, A. L., Pogozheva, I. D., and Mosberg, H. I. (2006) OPM: orientations of proteins in membranes database. *Bioinformatics 22*, 623−625.
(34) Jo, S., Kim, T., Iyer, V. G., and Im, W. (2008) CHARMM-GUI: a web-based graphical user interface for CHARMM. *J. Comput. Chem. 29*, 1859−1865.
(35) Brooks, B. R., Brooks, C. L., 3rd, Mackerell, A. D., Jr., Nilsson, L., Petrella, R. J., Roux, B., Won, Y., Archontis, G., Bartels, C., Boresch, S., Caflisch, A., Caves, L., Cui, Q., Dinner, A. R., Feig, M., Fischer, S., Gao, J., Hodoscek, M., Im, W., Kuczera, K., Lazaridis, T., Ma, J., Ovchinnikov, V., Paci, E., Pastor, R. W., Post, C. B., Pu, J. Z., Schaefer, M., Tidor, B., Venable, R. M., Woodcock, H. L., Wu, X., Yang, W., York, D. M., and Karplus, M. (2009) CHARMM: the biomolecular simulation program. *J. Comput. Chem. 30*, 1545−1614.
(36) Cheng, X., Jo, S., Lee, H. S., Klauda, J. B., and Im, W. (2013) CHARMM-GUI micelle builder for pure/mixed micelle and protein/micelle complex systems. *J. Chem. Inf. Model. 53*, 2171−2180.
(37) Maurya, S. R., Chaturvedi, D., and Mahalakshmi, R. (2013) Modulating lipid dynamics and membrane fluidity to drive rapid folding of a transmembrane barrel. *Sci. Rep. 3*, 1989.
(38) Gupta, A., Iyer, B. R., Chaturvedi, D., Maurya, S. R., and Mahalakshmi, R. (2015) Thermodynamic, structural and functional properties of membrane protein inclusion bodies are analogous to purified counterparts: case study from bacteria and humans. *RSC Adv. 5*, 1227−1234.
(39) Schlebach, J. P., Kim, M. S., Joh, N. H., Bowie, J. U., and Park, C. (2011) Probing membrane protein unfolding with pulse proteolysis. *J. Mol. Biol. 406*, 545−551.
(40) Leney, A. C., McMorran, L. M., Radford, S. E., and Ashcroft, A. E. (2012) Amphipathic polymers enable the study of functional membrane proteins in the gas phase. *Anal. Chem. 84*, 9841−9847.
(41) Lakowicz, J. R. (2009) *Principles of Fluorescence Spectroscopy*; Springer London, Limited, London.
(42) Maurya, S. R., and Mahalakshmi, R. (2013) Modulation of human mitochondrial voltage-dependent anion channel 2 (hVDAC-2) structural stability by cysteine-assisted barrel-lipid interactions. *J. Biol. Chem. 288*, 25584−25592.
(43) Moon, C. P., and Fleming, K. G. (2011) Using tryptophan fluorescence to measure the stability of membrane proteins folded in liposomes. *Methods Enzymol. 492*, 189−211.
(44) Moon, C. P., Zaccai, N. R., Fleming, P. J., Gessmann, D., and Fleming, K. G. (2013) Membrane protein thermodynamic stability may serve as the energy sink for sorting in the periplasm. *Proc. Natl. Acad. Sci. U. S. A. 110*, 4285−4290.
(45) Chaturvedi, D., and Mahalakshmi, R. (2014) Juxtamembrane tryptophans have distinct roles in defining the OmpX barrel-micelle boundary and facilitating protein-micelle association. *FEBS Lett. 588*, 4464−4471.
(46) Marks, D. S., Hopf, T. A., and Sander, C. (2012) Protein structure prediction from sequence variation. *Nat. Biotechnol. 30*, 1072−1080.
(47) Sheridan, R., Fieldhouse, R. J., Hayat, S., Sun, Y., Antipin, Y., Yang, L., Hopf, T., Marks, D. S., and Sander, C. (2015) *EVfold.org: Evolutionary Couplings and Protein 3D Structure Prediction*, DOI: 10.1101/021022.
(48) McMorran, L. M., Bartlett, A. I., Huysmans, G. H., Radford, S. E., and Brockwell, D. J. (2013) Dissecting the effects of periplasmic chaperones on the in vitro folding of the outer membrane protein PagP. *J. Mol. Biol. 425*, 3178−3191.
(49) Kleinschmidt, J. H., and Popot, J. L. (2014) Folding and stability of integral membrane proteins in amphipols. *Arch. Biochem. Biophys. 564*, 327−343.
(50) Calabrese, A. N., Watkinson, T. G., Henderson, P. J., Radford, S. E., and Ashcroft, A. E. (2015) Amphipols outperform dodecylmaltoside micelles in stabilizing membrane protein structure in the gas phase. *Anal. Chem. 87*, 1118−1126.
(51) Huysmans, G. H., Radford, S. E., Baldwin, S. A., and Brockwell, D. J. (2012) Malleability of the folding mechanism of the outer membrane protein PagP: parallel pathways and the effect of membrane elasticity. *J. Mol. Biol. 416*, 453−464.
(52) Bishop, R. E., Gibbons, H. S., Guina, T., Trent, M. S., Miller, S. I., and Raetz, C. R. (2000) Transfer of palmitate from phospholipids to lipid A in outer membranes of gram-negative bacteria. *EMBO J. 19*, 5071−5080.
(53) Jia, W., El Zoeiby, A., Petruzziello, T. N., Jayabalasingham, B., Seyedirashti, S., and Bishop, R. E. (2004) Lipid trafficking controls endotoxin acylation in outer membranes of *Escherichia coli*. *J. Biol. Chem. 279*, 44966−44975.
(54) Khan, M. A., Moktar, J., Mott, P. J., and Bishop, R. E. (2010) A thiolate anion buried within the hydrocarbon ruler perturbs PagP lipid acyl chain selection. *Biochemistry 49*, 2368−2379.
(55) Huysmans, G. H., Baldwin, S. A., Brockwell, D. J., and Radford, S. E. (2010) The transition state for folding of an outer membrane protein. *Proc. Natl. Acad. Sci. U. S. A. 107*, 4099−4104.
(56) Moon, C. P., and Fleming, K. G. (2011) Side-chain hydrophobicity scale derived from transmembrane protein folding into lipid bilayers. *Proc. Natl. Acad. Sci. U. S. A. 108*, 10174−10177.
(57) Santos, R. L., Zhang, S., Tsolis, R. M., Kingsley, R. A., Adams, L. G., and Baumler, A. J. (2001) Animal models of *Salmonella* infections: enteritis versus typhoid fever. *Microbes Infect. 3*, 1335−1344.
(58) Curnow, P., and Booth, P. J. (2007) Combined kinetic and thermodynamic analysis of alpha-helical membrane protein unfolding. *Proc. Natl. Acad. Sci. U. S. A. 104*, 18970−18975.
(59) Roy, A., Kucukural, A., and Zhang, Y. (2010) I-TASSER: a unified platform for automated protein structure and function prediction. *Nat. Protoc. 5*, 725−738.
(60) http://www.ebi.ac.uk/Tools/msa/clustalw2/.

DOI: 10.1021/acs.biochem.5b00543
Biochemistry 2015, 54, 5712−5722